AIChE Wiley InterScience DISCOVER SOMETHING GREAT

Particle Migration in the Rotating Flow Between Co-Axial Disks

Adetola A. Abatan and Joseph J. McCarthy
Dept. of Chemical and Petroleum Engineering, University of Pittsburgh, Pittsburgh, PA 15261

Watson L. Vargas
School of Engineering, Universidad Militar Nueva Granada, Bogota D.C., Colombia

DOI 10.1002/aic.10834
Published online March 27, 2006 in Wiley InterScience (www.interscience.wiley.com).

We experimentally examine a dilute suspension of non-neutrally buoyant spherical particles migrating in a simple mixing tank at small but finite Reynolds numbers. We observe that the particles spontaneously migrate to repeatable non-trivial asymptotic locations within toroidal structures, located above and below at-disk impellers. The asymptotic migration positions include both the exact center of the torus and intermediate higher-order cluster locations within the flow whose stability is dependent on flow and particle conditions. Furthermore, we note that the particle clusters seem to coincide with the location of unmixed islands within the underlying fluid flow. We also observe a migratory competition when multiple particles are introduced into the flow. © 2006 American Institute of Chemical Engineers *AIChE J,* 52: 2039–2045, 2006
Keywords: multiphase flow, stirred tank, particle migration, KAM, non-Brownian

Introduction

Multiphase flows are prevalent in various industrial applications, such as separations processes, catalysis, cell-growth bioreactors, and/or membrane filtration apparatus. Due to the interplay between phases, the characterization of such flows is rather complex yet necessary to fully understand the intrinsic dynamics of these processes.

Non-Brownian particles have long been observed to cross streamlines within a multiphase flow at rates significantly faster than by diffusion alone. Segre and Silberberg[1,2] first showed that neutrally buoyant particles can migrate across streamlines to non-trivial equilibrium positions within a uni-directional flow, regardless of their initial position(s). Subsequent work has shown that this phenomenon is quite general, being observed both experimentally and computationally in Poiseuille[3,4] and Couette[5-7] flows, and also as a function of particle density,[8,9] asphericity, and/or deformability.[10,11]

The cause of migration in these flows has largely been attributed to buoyancy effects[12,13] and/or non-linear fluid effects,[14-16] which arise at moderate Reynolds numbers; however, particle migration has also been observed in dense multiparticle flows even in the case of vanishing Reynolds number (that is, an ideal Stokes' flow). This is credited to hydrodynamic interactions between the particles[17] and termed "shear-induced migration." As we are primarily interested in the asymptotic behavior of dilute flows, this effect is beyond the scope of the research presented here.

Apparatus and Procedure

In this study we examine the migration of non-neutrally buoyant particles of a dilute suspension in a 1500 ml simple mixing tank with multiple 3 in. (38.1 mm) diameter flat-disk impellers equidistantly spaced along an axial shaft, as shown in Figure 1a. We built a co-axial stirred tank geometry as it represents a simple three-dimensional closed flow system where fluid drag may be used to counteract gravitational settling. This geometry, therefore, allows us to study the non-trivial asymptotic behavior of non-neutrally buoyant particles. By choosing a finite-sized cylindrical mixing tank, we are able to observe a competition between centrifugal buoyancy forces,

Correspondence concerning this article should be addressed to J. J. McCarthy at mccarthy@engrng.pitt.edu.

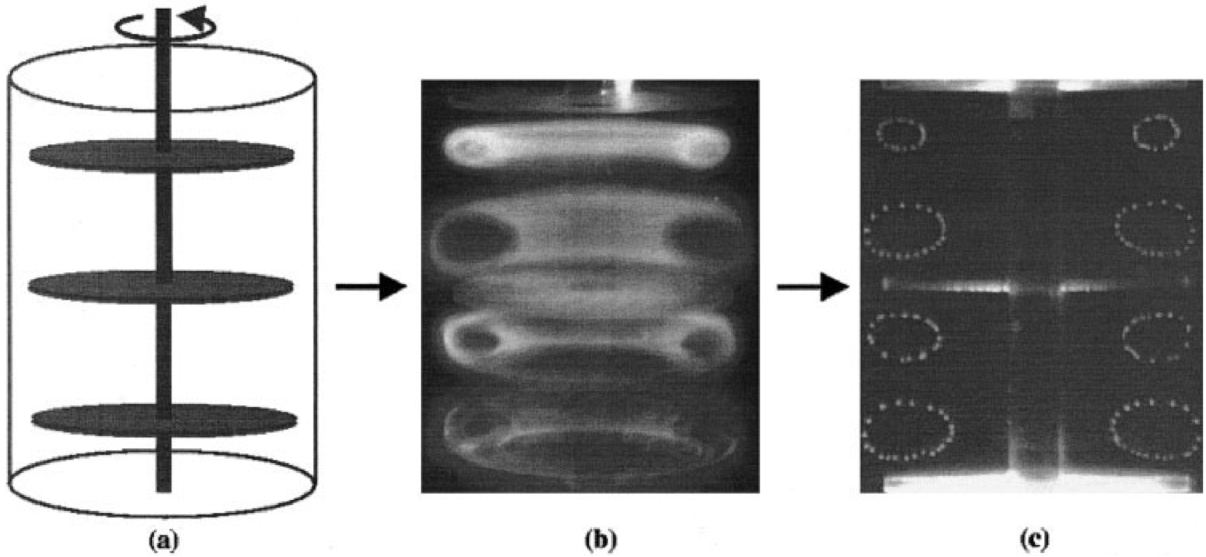

Figure 1. (a) Mixing tank geometry; (b) snapshot of fluid tori that form between adjacent impellers; (c) 60-s exposure of 2 mm particles tracing out cellular orbitals within the fluid tori.

wall interactions, and particle inertial effects, as a function of the local shear environment. As will be shown, this balance results in repeatable asymptotic locations within the flow. Moreover, the underlying mixing tendency of the flow—which can be made almost globally chaotic—seems to play a significant role in the migration behavior.

Mixing mechanisms within stirred tanks have been extensively studied, and the effects of geometric features (for example, the uniformity of the velocity field) have been examined.[18,19] It is known that the invariant fluid tori that form between impellers are separated by Kolmogorov-Arnold-Moser (KAM) surfaces, such that they are isolated from the outside flow and from each other except through molecular diffusion, as shown in Figure 1b.

Alvarez et al.[20] determined that the flow within a torus can be chaotic depending on the symmetry of the flow and the rotational protocol of the impeller(s). Similarly, Fountain et al.,[19,21] using both computational and experimental techniques, developed a theory for predicting regions of regularity (which are centered about elliptical points) and chaos (which contain hyperbolic points, and enhance mixing due to the stretching and folding of fluid elements) in a 3D flow. The authors called the non-chaotic regions "islands" and theorized that these were actually closed higher-order KAM surfaces/tori that twist around the tank at a different periodicity yet remain nested within the primary toroidal flow.

A 532 nm wavelength laser diode (purchased from Edmund Industrial Optics) equipped with a beam splitter is used to illuminate a 2-D cross-section of the tank. When particles are introduced into the steady state flow, a high resolution CCD camera placed perpendicular to the laser sheet is used to create stroboscopic maps of the particle location each time it crosses the two-dimensional plane. Using long exposure times, we are able to capture multiple crossings within the same frame, creating experimental Poincaré sections of the particle motion within individual cells. Figure 1c is an example of such toroidal cross-sections, where the exposure time is 60 s with approximately 20 particle crossings in each snapshot. This experimental snapshot is of four particles tracing out cellular orbitals at a rotation rate of 80 rpm and with a 2-in. (5.08 cm) impeller spacing.

In all experiments, the continuous phase is glycerin (S.G. = 1.26), whereas the slightly non-neutrally buoyant particles are either acrylic (S.G. ≅ 1.14) or cellulose acetate (S.G. ≅ 1.30) beads, 1.6 mm or 2 mm in diameter. Based on the density differences, the particles are identified as *light*, that is, density is slightly smaller than glycerin; or *heavy*, that is, density is slightly greater than glycerin.

By plotting the radial position of the particles as a function of time, we quantitatively measure the rate of migration for each particle. The reader should note that we choose particles that are large enough such that the effects of Brownian motion on individual particle trajectories are negligible and that migration rates are significant.

Observed Migration Patterns

Previous computational work[8,16] on the migration of very small particles within a cellular flow predicted that particles less dense than the continuous fluid phase moved inward toward the cell center, whereas more dense particles moved outward. In contrast, we have observed an inward migration for both heavier and lighter particles in the experiments reported here. The experimental snapshots of Figure 2 show typical

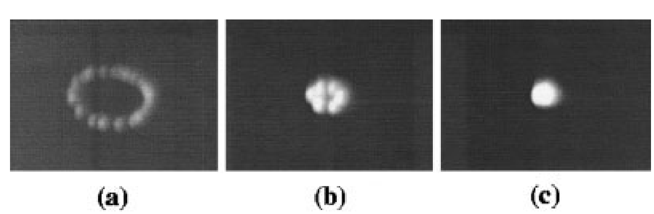

Figure 2. Experimental snapshots depict migration progress of a single particle at (a) 30 min, (b) 60 min, and (c) 90 min time intervals.

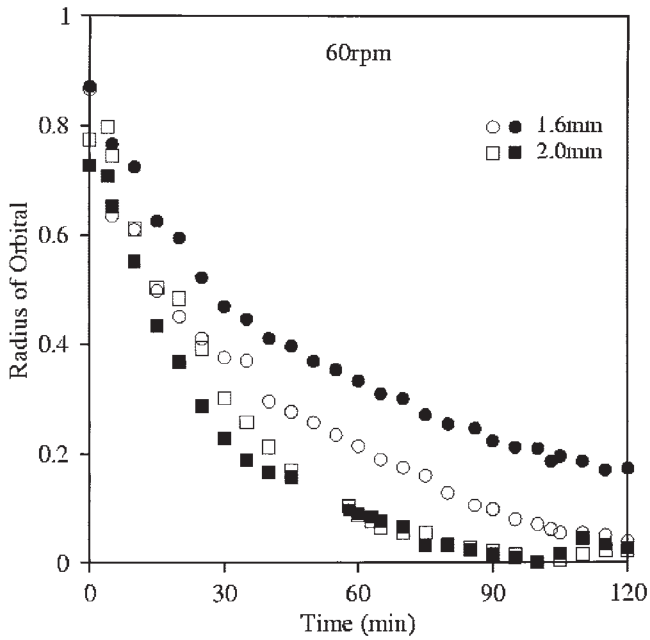

Figure 3. Migration rates for 1.6 mm and 2 mm particles at 60 rpm for a 2-in. (5.08 cm) spacing.

The smaller particles seem to migrate at a slower rate. Open symbols represent light particles; closed/filled symbols represent heavy particles.

circular trajectories for the monotonic inward migration of the particles. As the particle moves further within the cellular flow, the size of the circular path (that is, the radius of the particle orbital) decreases.

Asymptotic equilibria

We now examine the effects of particle size, rotation rate, and disk-spacing on the rate of migration. The reader should note that open symbols represent particles lighter than the fluid, whereas closed/filled symbols represent particles heavier than the fluid for all plots.

Figure 3 is a plot of the nondimensional radial position vs. time for 1.6 mm and 2 mm particles at 60 rpm. The migration rates of the light and heavy particles are relatively similar, especially as the size of the particle increases. This is likely due to the fact that the particles are within 10 percent difference from the density of glycerin. Another observation is that the slope of the 2 mm curve is steeper than for the 1.6mm particles; that is, it requires more time for the smaller particles to migrate across the same flow. It would seem that a smaller particle would tend to behave more like a tracer and be more susceptible to passive advection by the flow. However, that dependence decreases as the size of the particle increases.

By varying the distance between adjacent impellers as well as the impeller rotation rate, we can vary the local shear environment within the tori and observe the impact of these parameters on the particle migration process. The cell width (defined as the tank wall-to-shaft distance) is kept constant and used to non-dimensionalize the radial position of the particle as it migrates within the cross-sectional cellular flow. The cell height (defined as half of the disk-to-disk distance) changes as the spacing between adjacent impellers is varied from 2-4 in. (5.08-10.16 cm).

The spacing between adjacent parallel disks affects the size of the toroidal structures, which in turn affects the migration rate of the particles. This is quantitatively depicted in Figure 4, which shows that for different rotation rates, 2 mm slightly non-neutrally buoyant particles—both lighter and heavier—migrate inwards following a loosely exponential curve toward the torus center. Based on the data in Figure 4, there seems to be an increase in migration rate with impeller spacing, requiring at least 90 min for the migration to $r = 0$ for the 2-in. spacing vs. 60 min for the 3-in. spacing experiments. This was

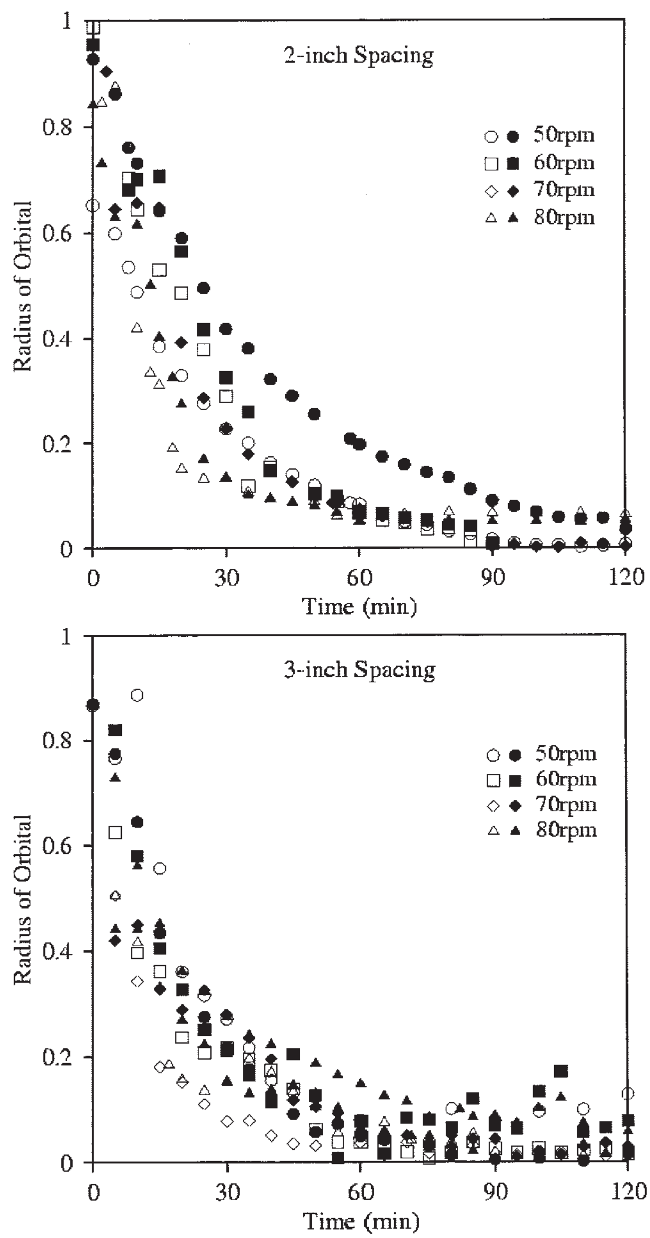

Figure 4. Radial position for 2 mm particles as a function of time at different rotation rates (50-80 rpm) and impeller spacings (2-3 in.).

Both light particles and heavy particles migrate inwards.

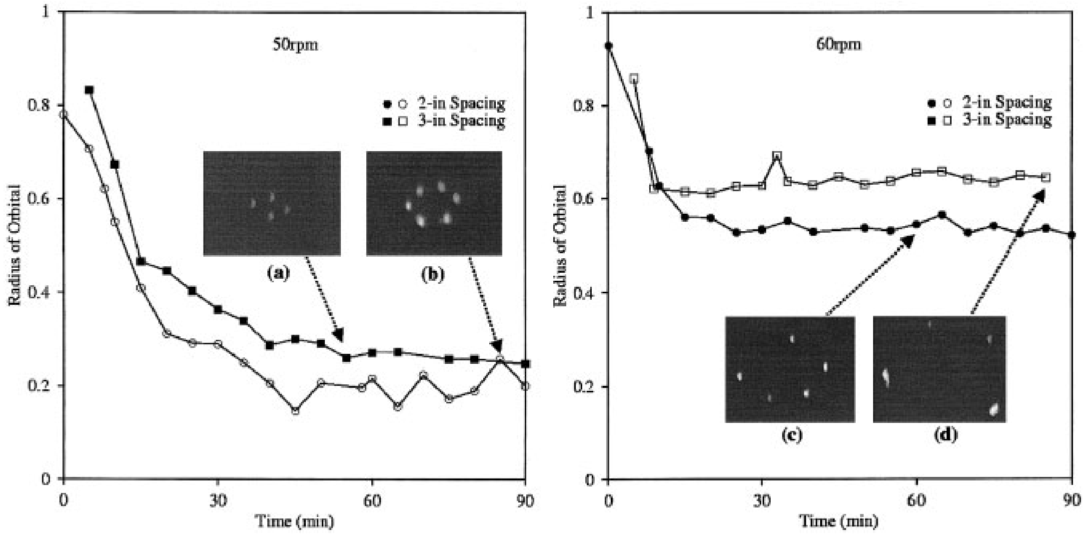

Figure 5. Radial particle positions, illustrating linear progression until clusters are formed.

Inset snapshots illustrate: (a) 50 rpm, 3-in. spacing, period 4; (b) 50 rpm, 2-in. spacing, period 6; (c) 60 rpm, 3-in. spacing, period 5; (d) 60 rpm, 2-in. spacing, period 4.

also confirmed for the 4-in. spacing, although those data are not shown. It would seem that as the impeller and shaft rotation rate increases, the rate of migration increases correspondingly.

Nontrivial asymptotic equilibria

As previously stated, particles typically trace out relatively circular paths while gradually spiraling inwards within the fluid torus. For some particles, however, the crossings occur at the same radial positions, creating "clusters." The experiments were usually allowed to run for at least 2 hours; thus, for prolonged periods of time, the particle continuously crosses the 2-D plane in a small number of discrete locations and inward migration ceases. We designate the center of the cell/torus as a period 1 cluster, that is, all particle crossings occur at a single location. In a similar manner, a period *n* cluster means that the particle crosses the 2-D plane in *n* discrete locations. It is worth noting that we observe cluster formations for both types of non-neutrally buoyant particles.

Figures 5 and 6 show some of the cluster patterns we have observed and the orbital radius at which they occur. Again, open symbols represent light particles and closed/filled symbols represent heavy particles. The inset snapshots illustrate the particle orbital at the times indicated, as well as some of the various cluster formations we have observed. Table 1 concisely displays the observed cluster patterns, as well as the approximate asymptotic value of the radial position. Recall that each snapshot contains roughly 20 particle crossings.

At 50 rpm, we observe inward migration until the particles

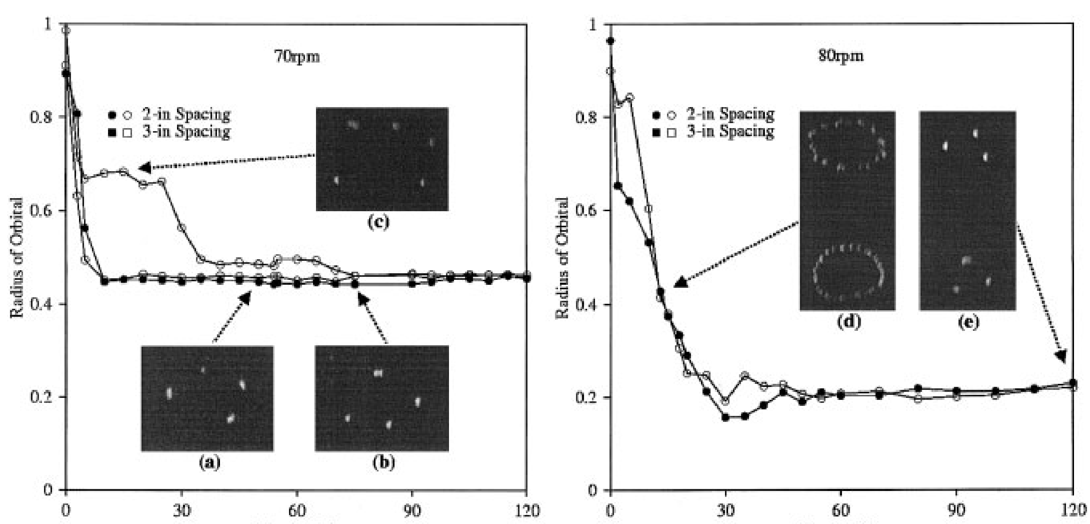

Figure 6. Radial particle positions.

Inset snapshots illustrate: (a,b) 70 rpm, 2-in. spacing, period 4; (c) 70 rpm, 2-in. spacing, period 5 (quasi-stable at this rotation rate); (d) 80 rpm, 2-in. spacing, regular crossings; (e) 80 rpm, 2-in. spacing, period 3 for both a light (top) and heavy (bottom) particle.

Table 1. **Periodicity of Particle Clusters for 2- and 3-in. Spacing as a Function of Rotation Rate**

RPM	2-in. Spacing		3-in. Spacing	
	Clusters	Radius	Clusters	Radius
50	6	0.25	4	0.20
60	5	0.55	4	0.65
70	4	0.45	5	0.61*
80	3	0.20	—	—

Note: The period 5 cluster observed at 70 rpm (radius = 0.61) was seen for approximately 35 min; others were stable for the duration of the experiments.

reach a period 4 formation for the 3-in. spacing (Figure 5a) and a period 6 formation for the 2-in. spacing (Figure 5b). The 60 rpm plot displays a period 5 formation for the 2-in. spacing (Figure 5c) and a period 4 formation for the 3-in. spacing (Figure 5d). However, the shape and radial position of these clusters are at a higher radial position than for the 50 rpm data (see Table 1).

For the 70 rpm plot, we observe two different period 4 formations in Figures 6a and 6b. Figure 6a especially bears resemblance to the period 4 cluster observed at 60 rpm in Figure 5d. However, we also observe a quasi-stable period 5 formation (Figure 6c) for approximately 25 min before the particle migrates further inward and stalls in a period 4 formation similar to the other particles. A different period 5 formation was also seen at 70 rpm but for a 3-inch spacing and was maintained for approximately 35 min (not shown, but detailed in Table 1). At 80 rpm, we note that the slope of the curves monotonically decreases when the particle crossings are distinct and separate, as seen in Figure 6d. In contrast, the curves level off when the particle crossings cluster into a period 3 formation (Figure 6e) and the particle migration stalled.

For the particle and flow conditions studied, it would seem that the stability of the clusters is highly dependent on rotation rate and impeller spacing. When the particle exhibits cluster formations, we generally observe low-period stable clusters at lower radial positions with increased rotation rate, for example, period 5 clusters at 60 rpm vs. period 3 clusters at 80 rpm. An increase in impeller spacing also seems to yield lower-period formations, for example, period 5 clusters for a 2-in. spacing vs. period 4 for a 3-in. spacing at 60 rpm (see Table 1). From these results, it would seem that the radial position also increases since the higher-order clusters are located further away from the cell center.

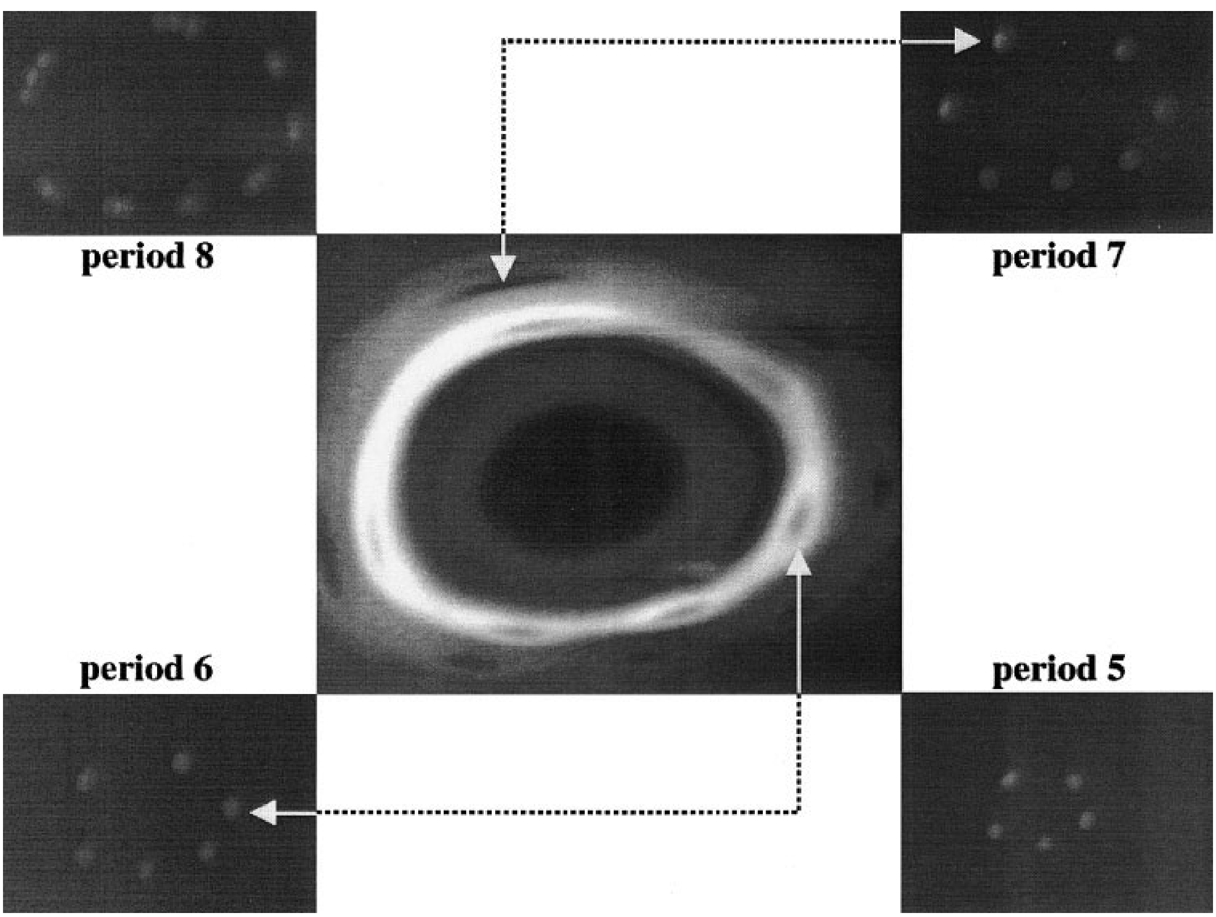

Figure 7. Higher-order cluster formations for both light and heavy particles, and the nested fluid islands that cause the stalling behavior.

The arrows clearly indicate the period 6 and period 7 islands, as well as the corresponding particle position in the cluster formations. Rotation rate is 60 rpm.

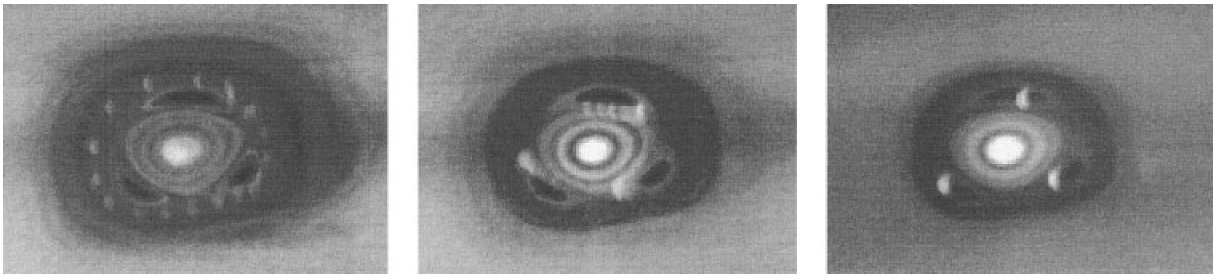

Figure 8. Dye advection snapshots of a heavy particle at 80 rpm.

(Left) linear migration when the particle is between KAM surfaces; (middle) interaction with the KAM tube, which manifests as a clustering of particle positions in the 2-D laser sheet; (right) particle is trapped within the fluid islands, creating a period 3 cluster.

Particle-fluid hydrodynamics

To clarify the effect of the mixing on the particle motion, we performed dye-advection experiments using Rhodamin B fluorescent dye. Figure 7 illustrates both period 6 and 7 island chains within the same flow, as well as the corresponding particle migration clusters of the same periodicity. The period 5 and 8 clusters are shown for completion. These experiments show that the chaotic flow is made up of nested island chains of decreasing periodicity as one moves towards the center of the fluid torus.

Figure 8 combines dye advection and particle migration to further illustrate that the locations of these clustered crossings seem to exactly coincide with regular regions (islands) within the chaotic flow, as suggested in Figure 7. The particle crossings remain discrete (separated) when the particle is outside of these islands, yet are clustered in these periodic islands when the particle is stalled within the previously-mentioned KAM tubes or higher-order islands. The period 3 islands in Figure 8c very closely mirror the 80 rpm experiment in Figure 6. It would seem that migration mechanisms dominate in the well-mixed regions of the primary flow; thus, the observed particle motion is monotonic. In contrast, in regions where the isolated fluid islands are stable, the migration is thwarted and the motion of the particles is halted in the various cluster formations shown.

The dye-advection snapshots illustrate the importance of the size of the unmixed island chains relative to the particle diameter. Assuming the sizes of the higher-order islands increase as the particle approaches the torus center,[19,21] then larger particles are forced to migrate further inward to find islands that are large enough to be trapped within. However, if the sizes of the fluid islands are preserved by an increased impeller spacing, the particle can still reside in a higher-period island at a relatively higher rotation rate. This would help to explain the same periodicity clusters at different rotation rates and different impeller spacings that we observe in Table 1.

Multiparticle competition

As more particles are added to a suspension, inter-particle interactions become a matter of interest. While the flow still remains largely dilute, even the addition of a second particle forces particles to "compete" for the asymptotic positions, as shown in Figure 9. The 70 and 80 rpm plots compare two heavy particles with the progress of a single heavy particle.

Both particles occupy the same circular path at the beginning

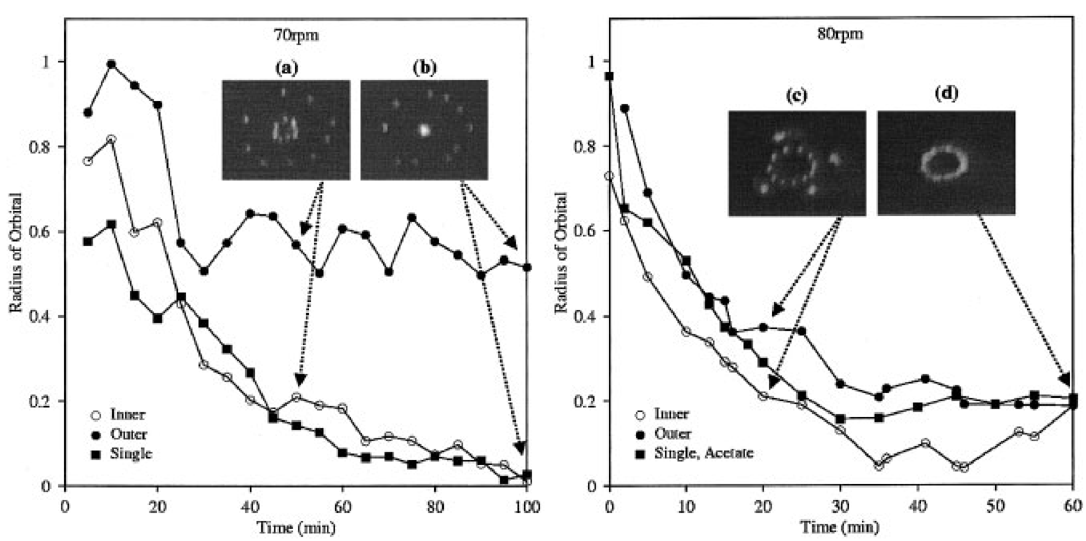

Figure 9. Comparison of radial positions for the two competing particles and a single particle at the same rotation rate.

Inset snapshots were taken after: 70 rpm- (a) 50 min and (b) 100 min; 80 rpm- (c) 20 min and (d) 60 min. Experiments show the inner particle migrating in a similar manner to a single particle, while the outer maintains an outer orbital or cluster formation.

of the 70 rpm experiment. However, one particle overcomes the centrifugal forces and migrates inward, whereas the other maintains an outer orbital (Figure 9a). Closer examination of the radial positions shows that the motion of the *inner* particle is similar to that of a single particle experiment at the same rotation rate. In contrast, the *outer* particle stalls at a radial position $\cong 0.55$, where its attempts to move inward towards a period 1 position are hindered by the inner particle's presence (Figure 9b).

Cluster formation is still observed for competing particles. The 80 rpm plot of Figure 9 shows the outer particle clearly tracing out a period 4 formation (Figure 9c) for approximately 10 min of the experiment, even as the inner particle (Figure 9d) remains discrete and monotonic in its migration. Eventually, the migration paths of both particles merge into a single cellular orbital.

Conclusions

We experimentally examined the migration phenomena within multiphase systems in order to understand and perhaps manipulate them to produce spontaneously-organized structured suspensions. Our results demonstrate that the migration of particles in a multi-directional, viscous flow with finite fluid inertia yields a rich variety of behavior. We find that particles both heavier and lighter than the continuous phase can migrate across streamlines to position themselves in repeatable equilibrium locations, in very similar manner. At certain rotation rates, we find that particles remain stalled in clusters within the flow for extended periods of time, which seem to closely coincide with regular islands within the chaotic fluid flow. This suggests that control of the asymptotic particle position is possible through manipulation of the fluid island positions. We also note that in two-particle experiments, interparticle interactions seem to promote/allow migration for one particle at the expense of the other even at vanishingly small concentrations. These findings could potentially impact a wide variety of applications in the environmental, bioengineering, and materials science fields.

Acknowledgments

We wish to acknowledge Mr. Armin W. Opitz and Ms. Eyma Y. Marrero for performing initial experiments. This work was funded by the National Science Foundation (CTS-0105688) and the Department of Energy (DE-FG26–02NT41554).

Literature Cited

1. Segré G, Silberberg A. Radial particle displacements in poiseuille flow of suspensions. *Nature.* 1961;189:209-210.
2. Segré G, Silberberg A. Behavior of macroscopic rigid spheres in poiseuille flow. *Journal of Fluid Mechanics.* 1962;14:115-156.
3. Vasseur P, Cox RG. The lateral migration of a spherical particle in two-dimensional shear flow. *Journal of Fluid Mechanics.* 1976;78:385-393.
4. Cox RG, Nadim A, Brenner H. Transport of sedimenting brownian particles in a rotating poiseuille flow. *Physics of Fluids.* 1985;28:3457-3466.
5. Halow JS, Wills GB. Radial migration of spherical particles in couette system. *AIChE J.* 1970;16:281-286.
6. Chan CC, Fung JCH. The change in settling velocity of inertial particles in cellular flow. *Fluid Dynamics Research.* 1999;25:257-273.
7. Mauri R, Papageorgiou DT. The onset of particle segregation in plane couette flows of concentrated suspensions. *Int J Multiphase Flows.* 2002;28:127-136.
8. Crisanti A, Falcioni M, Provenzale A, Vulpiani A. Passive advection of particles denser than the surrounding fluid. *Physics Letters A.* 1990;150(2):79-84.
9. Ye J, Roco MC. Particle rotation in a couette flow. *Physics of Fluids A.* 1992;4:220-224.
10. Schiek RL, Shaqfeh EG. Cross streamline migration of slender brownian fibres in plane poiseuille flow. *J Fluid Mechanics.* 1997;332:23-39.
11. Magnaudet J. Small inertial effects on a spherical bubble, drop or particle moving near a wall in a time-dependent linear flow. *J Fluid Mechanics.* 2003;485:115-142.
12. Ho BP, Leal LG. Inertial migration of rigid spheres in two-dimensional uni-directional flows. *J Fluid Mechanics.* 1974;65:365-400.
13. Morris JF, Brady JF. Pressure-driven flow of a suspension: buoyancy effects. *Int J Multiphase Flows.* 1998;24:105-130.
14. Saffman PG. The lift on a small sphere in a slow shear flow. *J Fluid Mechanics.* 1965;22:385-398.
15. Mctigue RF, Givler RC, Nunziato JW. Rheological effects of non-uniform particle distributions in dilute suspensions. *J Rheology.* 1986;30:1053-1076.
16. Maxey MR. The motion of small spherical particles in a cellular flow field. *Physics of Fluids.* 1987;30:1915-1928.
17. Leighton D, Acrivos A. The shear-induced migration of particles in concentrated suspensions. *J Fluid Mechanics.* 1987;181:415-439.
18. Lamberto DJ, Muzzio FJ, Swanson PD. Using time-dependent rpm to enhance mixing in stirred vessels. *Chem Eng Sci.* 1996;51(5):733-741.
19. Shinbrot T, Alvarez MM, Zalc JM, Muzzio FJ. Attraction of minute particles to invariant regions of volume preserving flows by transients. *Phys Rev Lett.* 2001;86(7):1207-1210.
20. Alvarez MM, Zalc JM, Shinbrot T, Muzzio FJ. Mechanisms of mixing and creation of structure in laminar stirred tanks. *AIChE J.* 2002;48:2135-2148.
21. Fountain GO, Khakar DV, Mezic I, Ottino JM. Chaotic mixing in a bounded three-dimensional flow. *J Fluid Mechanics.* 2000;417:265-301.

Manuscript received Aug. 23, 2005, and revision received Feb. 20, 2006.